Journal of Remote Sensing
A SCIENCE PARTNER JOURNAL

RESEARCH ARTICLE

A General and Effective Method for Wall and Protrusion Separation from Facade Point Clouds

Shangshu Cai[1,2], Shuhang Zhang[1,2*], Wuming Zhang[1,2], Hongchao Fan[3], Jie Shao[1,2], Guangjian Yan[4], Sisi Yu[5], Aiguang Li[1,2], and Guoqing Zhou[6]

[1]School of Geospatial Engineering and Science, Sun Yat-Sen University, Guangzhou, China. [2]Southern Marine Science and Engineering Guangdong Laboratory (Zhuhai), Guangdong, China. [3]Department of Civil and Environmental Engineering, Norwegian University of Science and Technology, Trondheim, Norway. [4]Faculty of Geographical Science, Beijing Normal University, Beijing, China. [5]University of Chinese Academy of Sciences, Beijing, China. [6]Guilin University of Technology, Guilin, China.

*Address correspondence to: zhangsh52@mail.sysu.edu.cn

Citation: Cai S, Zhang S, Zhang W, Fan H, Shao J, Yan G, Yu S, Li A, Zhou G. A General and Effective Method for Wall and Protrusion Separation from Facade Point Clouds. *J. Remote Sens.* 2023;3:Article 0069. https://doi.org/10.34133/remotesensing.0069

Submitted 20 March 2023
Accepted 19 July 2023
Published 16 August 2023

As a critical prerequisite for semantic facade reconstruction, accurately separating wall and protrusion points from facade point clouds is required. The performance of traditional separation methods is severely limited by facade conditions, including wall shapes (e.g., nonplanar walls), wall compositions (e.g., walls composed of multiple noncoplanar point clusters), and protrusion structures (e.g., protrusions without regularity, repetitive, or self-symmetric features). This study proposes a more widely applicable wall and protrusion separation method. The major principle underlying the proposed method is to transform the wall and protrusion separation problem as a ground filtering problem and to separate walls and protrusions using ground filtering methods, since the 2 problems can be solved using the same prior knowledge, that is, protrusions (nonground objects) protrude from walls (ground). After transformation problem, cloth simulation filter was used as an example to separate walls and protrusions in 8 facade point clouds with various characteristics. The proposed method was robust to the facade conditions, with a mean intersection over union of 90.7%, and had substantially higher accuracy compared with the traditional separation methods, including region growing-, random sample consensus-, multipass random sample consensus-based, and hybrid methods, with mean intersection over union values of 69.53%, 49.52%, 63.93%, and 47.07%, respectively. Besides, the proposed method was general, since existing ground filtering methods (including the maximum slope, progressive morphology, and progressive triangular irregular network densification filters) can also perform well.

Introduction

Advanced 3-dimensional (3D) semantic facade models play an important role in damage assessment, urban planning, virtual reality, and energy management, among other applications [1–10]. Ground-based light detection and ranging (LiDAR) is the most accurate and detailed technology to represent the 3D structural information of facades, and semantic facade modeling is mainly based on ground-based LiDAR point clouds [11–22]. In the facade modeling, facade elements are hierarchically modeled, that is, walls and protrusions are separated, and their elements (e.g., windows and doors of walls and balconies and pipelines of protrusions) are modeled respectively. However, accurately separating walls and protrusions has been a huge challenge for complex facade conditions, including wall shapes (e.g., nonplanar walls), wall compositions (e.g., walls composed of multiple noncoplanar point clusters), and protrusion structures (e.g., protrusions without regularity, repetitive, or self-symmetric features). Therefore, it is crucial to develop a wall and protrusion separation method that can cope with various facade conditions.

Walls and protrusions usually are separated by wall detection methods because the prior knowledge of walls is easier to be generalized because of the simpler geometry compared to protrusions. We categorized wall detection methods as segmentation- and geometric fitting-based methods. The segmentation-based methods firstly segment facade point clouds and then identify the walls and protrusions based on the prior knowledge of walls. The segmentation groups points belonging to the same surface according to geometric constraints, such as smoothness, flatness, or completeness [23]. Multiple segmentation algorithms can be used, such as region growing- and clustering-based methods (e.g., *k*-means and fuzzy *C*-means) [24]. The region growing-based methods are easy to implement and preserve the boundary of objects [23]. The advantage of the clustering-based methods is that seeds are not required for initiating the grouping [24]. Nevertheless, the clustering-based methods are rarely used in wall and protrusion separation, probably due to expensive computation [24]. Both types of methods are highly affected by data quality, such as data missing [23–25]. Segments are classified using the rules, such as object size, orientation, topology, and location

[25]. For example, facade point clouds are segmented using the region growing method, and then wall segments are identified according to the prior knowledge that walls are large-sized, smooth, and perpendicular to ground [26]. However, the method is prone to misidentify large-sized protrusions as walls. Besides, the wall segments may also be misidentified as protrusions, when walls are segmented into multiple small-sized segments due to variable point densities [27,28].

The geometric fitting-based methods identify the wall points based on the prior knowledge that a wall is a plane. Many plane fitting methods [e.g., the random sample consensus (RANSAC) and Hough transform methods] are applied for wall detection, and RANSAC is the most widely used method. In the method, a series of plane model proposals are generated by randomly sampling data points in a facade point cloud, and the model with the most numerous inliers is adopted [16,19,29]. The model fitting-based methods can completely identify the walls composed of coplanar plane points. However, it has difficulty in the detection of free-form walls, such as noncoplanar planar and nonplanar walls [30].

Li et al. [18] proposed a hybrid method by combining the segmentation- and geometric fitting-based methods. The hybrid method first segments facade point clouds and then fits plane based on the largest segments. Finally, the segments within the plane buffer are identified as walls. The method can completely identify walls while preventing the generation of false planes. However, the noncoplanar planar and nonplanar wall detection are still challenging for the hybrid-based method.

In addition to wall detection methods, walls and protrusions can also be separated using protrusion detection methods, which are developed on the basis of the prior knowledge that protrusions are regularity, repetitive, or self-symmetric [17,31,32]. For example, Friedman and Stamos [32] formulated a function using a geometric feature of each point and clarified the periodical features to identify repetitive protrusions using the Fourier transform method. However, the method is only available in the facades with the above structured protrusions.

In summary, the performance of the published methods is limited by facade conditions, including wall shapes, wall compositions, and protrusion structures. To overcome the

Table 1. Characteristics and statistics of all facades.

Samples	Wall shapes	Wall compositions	Protrusion conditions	Proportion of protrusions (%)	Reference (points)	
					Walls	Protrusions
Facade 1	Planar	Multiple coplanar planar parts	Windows with small protruding depths	42.67	23,762	17,685
Facade 2	Planar	Multiple noncoplanar planar parts	Advertising boards, air conditioner outer units and pipelines with different protruding depths	31.91	35,269	16,532
Facade 3	Planar	Multiple noncoplanar planar parts	Balconies, windows and beam with different protruding depths	57.09	14,288	19,009
Facade 4	Curved	Multiple nonplanar parts	Sun shield with large protruding depths	0.81	84,684	690
Facade 5	U	Multiple coplanar planar and multiple noncoplanar planar parts	Sun shield and beam with large protruding depths	27.96	50,437	19,578
Facade 6	Spoon	Multiple coplanar planar, multiple noncoplanar planar and multiple nonplanar parts	Windows and beam with different protruding depths	29.85	14,909	6,343
Facade 7	Saddle	Multiple coplanar planar and multiple nonplanar parts	Balconies, windows with small protruding depths	43.6	85,862	66,379
Facade 8	Spoon	Multiple coplanar planar, multiple noncoplanar planar and multiple nonplanar parts	Windows and beam with small protruding depths	36.88	81,377	47,551

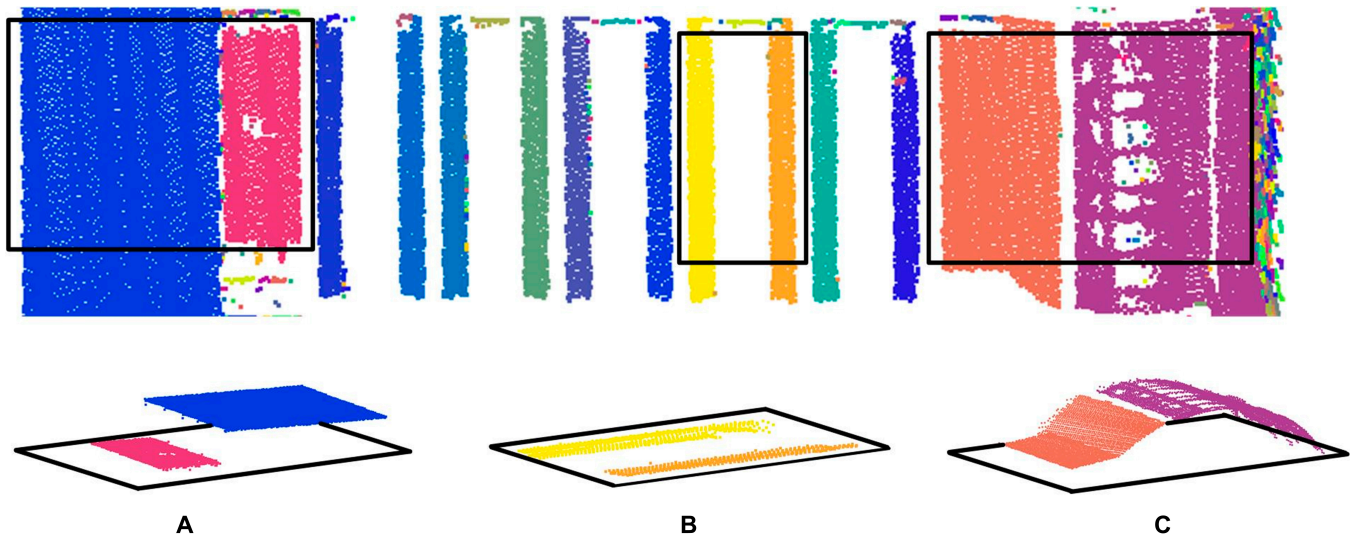

Fig. 1. Examples of different wall compositions: (A) multiple noncoplanar planar parts, (B) multiple coplanar planar parts, and (C) multiple nonplanar parts.

limitation, this study proposes a novel wall and protrusion separation method. The main principle of the proposed method is to transform the wall and protrusion separation problem as a ground filtering problem and to separate walls and protrusions using existing ground filtering methods. The proposed method has the following advantages: (a) The complexity of facade seldom influences wall and protrusion separation because the used prior knowledge (i.e., protrusions protrude from walls) is independent of wall shapes, wall compositions, and protrusion structures; (b) walls and protrusions can be accurately separated by existing ground filtering methods, which have effective rules corresponding to the knowledge.

Following Introduction, Materials and Methods section provides a detailed description of the tested data and the proposed method. The proposed method is validated and discussed in Results and Discussion sections. Finally, the conclusions and future work are drawn in the Conclusion section.

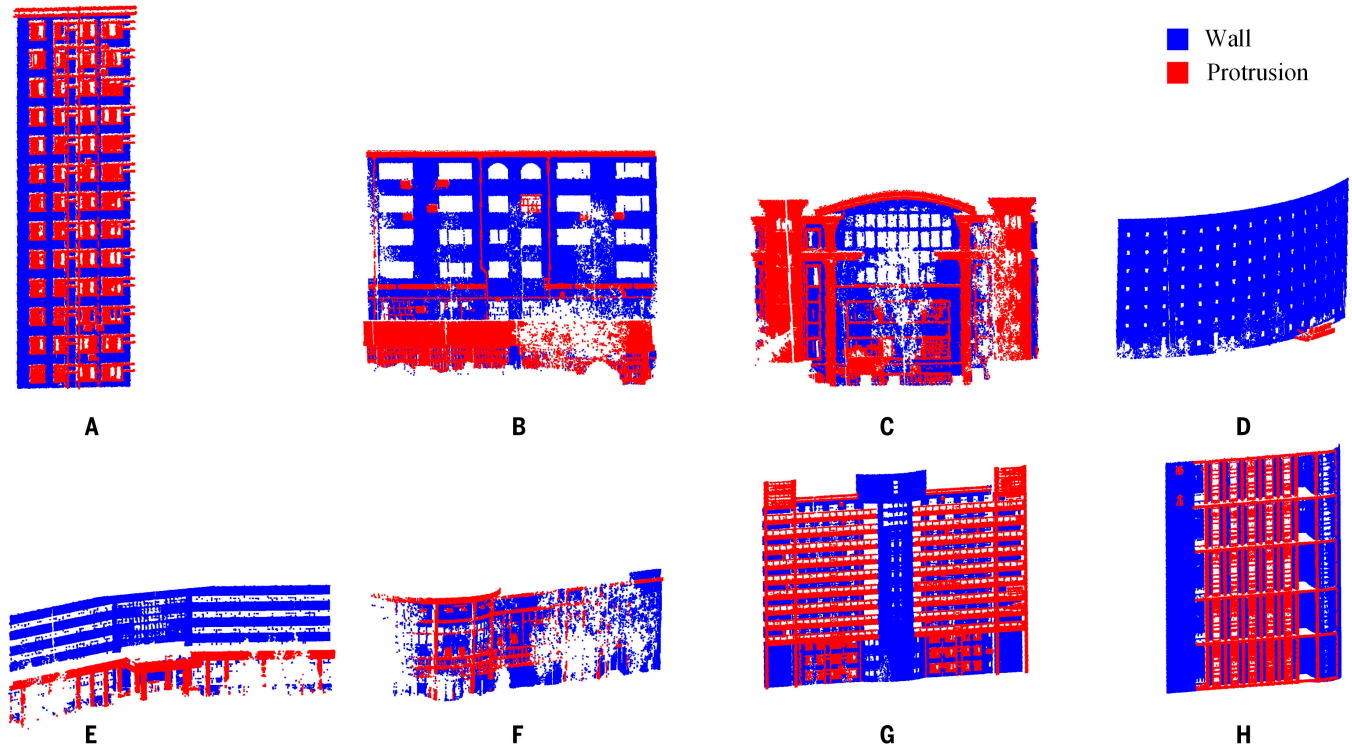

Fig. 2. All facade point clouds: (A to H) facades 1 to 8.

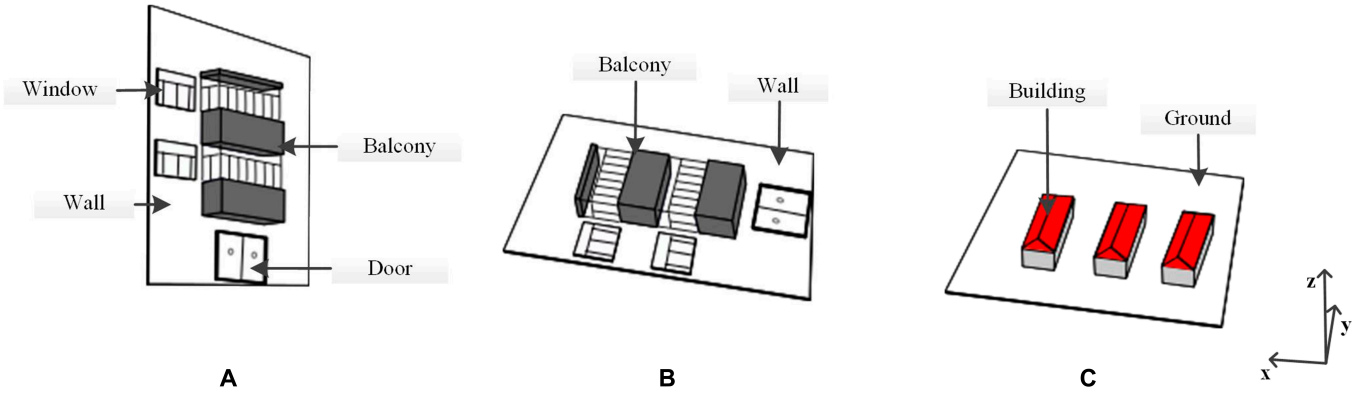

Fig. 3. Conceptual diagrams of the proposed wall and protrusion separation method. (A) The standing facade is converted to (B) a natural-like scene. The wall and the protrusions (i.e., balconies) in the natural-like scene are equivalent to the ground and the nonground objects (i.e., buildings) in (C) the natural scene. Thus, the wall and the protrusions in the natural-like scene can be separated by ground filtering methods.

Materials and Methods

Data

Eight facades (named as facades 1 to 8) with different wall and protrusion conditions were used to evaluate the performance of the proposed method. The characteristics and statistics of wall and protrusion conditions for each facade are given in Table 1. The walls include planar, curved, U, spoon, and saddle shapes. The facades with planar and nonplanar wall shapes are grouped as simple and complex facades. The walls of facade 1 and facades 2 and 3 consist of coplanar planar and noncoplanar planar parts, respectively. Coplanar planar, noncoplanar planar, and nonplanar parts are included in the walls of facades 5 to 8. Figure 1 shows different wall compositions, including coplanar planar, noncoplanar planar, and nonplanar parts, using the partial wall of facade 8 as an example. The 8 facades contain a wide variety of protrusions, such as windows, advertising boards, and balconies. These protrusions have varied and complex structures, and their proportions in facades are obviously different, with proportion values of 0.81% to 57.09%. The ground-based LiDAR point clouds have different levels of data missing due to occlusion effects, with an average point spacing of 0.1 m. We generated the reference data by human–machine interaction. Figure 2 shows the reference data of all facades, in which wall and protrusion points are colored blue and red, respectively.

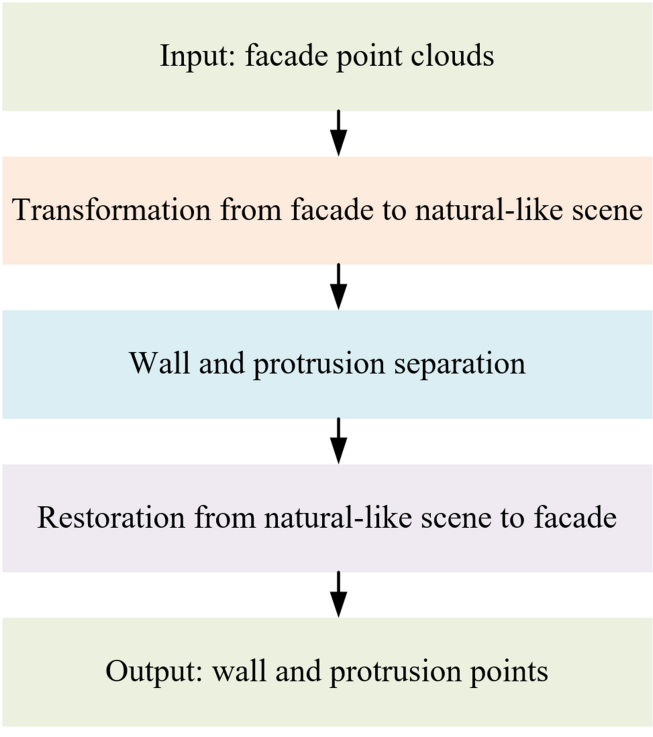

Fig. 4. Workflow of the proposed method.

Overview of the proposed method

Although the prior knowledge that protrusions protrude from walls is widely known and reliable for wall and protrusion separation, it seldom applied since the rules corresponding to the knowledge have not yet been reported. To overcome the limitation, we converted the wall and protrusion separation problem as a ground filtering problem and used ground filtering methods to separate walls and protrusions. As shown in Fig. 3, the facade is transformed to a natural-like scene, in which the wall and the protrusions (i.e., balconies) correspond to the ground and the nonground objects (i.e., buildings), respectively. As a result, existing ground filtering methods can be used to separate the wall and the protrusions in the natural-like scene. The transformation is necessary for utilizing ground filtering methods. The protruding direction of protrusions is free in 3D space, but the rules of ground filtering methods are designed on the basis of the z-axis direction, i.e., the protruding direction of nonground objects. The rules are invalid if protruding direction of protrusions is not consistent with the z-axis direction.

The workflow of the proposed method consists of 3 steps, i.e., transformation from facade to natural-like scene, wall and protrusion separation, and restoration from natural-like scene to facade (Fig. 4), which are described in the Transformation from facade to natural-like scene, Wall and protrusion separation, and Restoration from natural-like scene to facade sections.

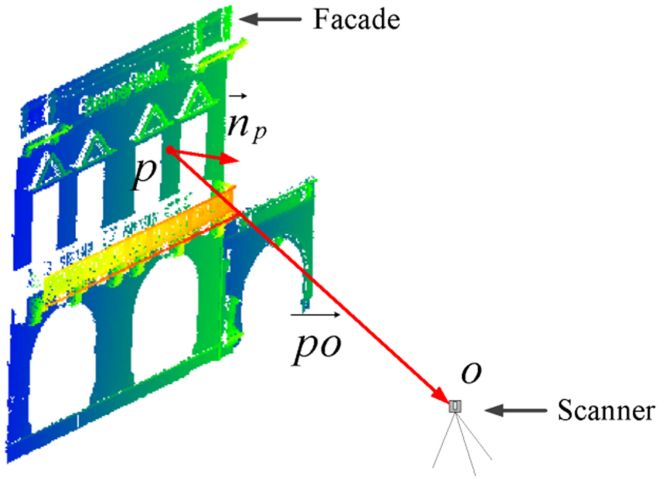

Fig. 5. Simple demonstration of determining normal vector orientation of a facade point. The normal vector orientation at the point p is determined by judging whether the normal vector $\overrightarrow{n_p}$ of p points toward the laser scanner origin o. If the dot product between $\overrightarrow{po}$ and $\overrightarrow{n_p}$ is positive, the orientation of $\overrightarrow{n_p}$ remains unchanged; otherwise, opposite orientation is adopted.

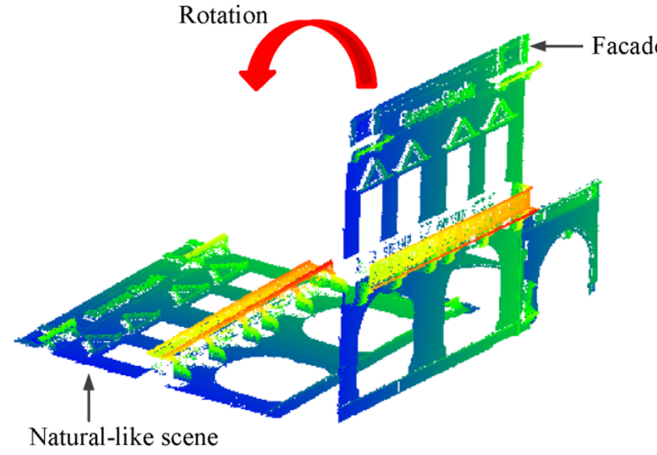

Fig. 6. An example of the facades before and after rotation. The facade is transformed to the natural-like scene, in which the wall and the protrusions are equivalent to the ground and the nonground objects, respectively.

Transformation from facade to natural-like scene

The facade is transformed into a natural-like scene, where protrusions protrude from walls in the z-axis direction. The transformation is implemented by rotating the normal vector of a facade to align with the z axis. The normal vector is defined as the average normal vector of all facade points. The normal vector of a facade point p is estimated using the principal components analysis method. The covariance matrix C of the neighbor points of p is calculated as Eq. 1 [33,34].

$$C = \frac{1}{N}\sum_{i=1}^{N}\left(p_i - \overline{p}\right)\left(p_i - \overline{p}\right)^T \tag{1}$$

where $\{p_i\}_{i=1:N}$ is the neighbor points corresponding to p and $\overline{p} = \frac{1}{N}\sum_{i=1}^{N} p_i$ is the centroid of neighbor points. The normal vector at p is estimated by the eigenvector of the smallest eigenvalue of C. The neighbor points are obtained through the k-nearest neighbor method.

The normal vector orientation of each facade point calculated by principal components analysis is inconsistent. It is unified using the line of sight information from a laser scanner. As shown in Fig. 5, the vector $\overrightarrow{po}$ from the facade point p to the laser origin o is determined. If the dot product between $\overrightarrow{po}$ and the normal vector $\overrightarrow{n_p}$ of p is positive, the orientation of $\overrightarrow{n_p}$ remains unchanged; otherwise, it is reversed, i.e., $\overrightarrow{n_p} = -\overrightarrow{n_p}$. After determining the normal vector orientation of all facade points, their average is regarded as facade normal vector $\overrightarrow{n_p}$.

On the basis of $\overrightarrow{n}_b$ and the vertical normal vector $\overrightarrow{n_z}$, the rotation matrix R for the transformation from facade to natural-like scene is calculated as Eq. 2.

$$R = \begin{bmatrix} \cos\theta y & 0 & \sin\theta y \\ 0 & 1 & 0 \\ -\sin\theta y & 0 & \cos\theta y \end{bmatrix}\begin{bmatrix} 1 & 0 & 0 \\ 0 & \cos\theta x & -\sin\theta x \\ 0 & \sin\theta x & \cos\theta x \end{bmatrix} \tag{2}$$

where θx and θy denote the rotation angles around the x and y axes, respectively. They are calculated as follows.

$$\theta x = \cos^{-1}\left[\frac{(y_b, z_b)\cdot(y_z, z_z)}{\left(\sqrt{y_b^2 + z_b^2}\right)\times\left(\sqrt{y_z^2 + z_z^2}\right)}\right] \tag{3}$$

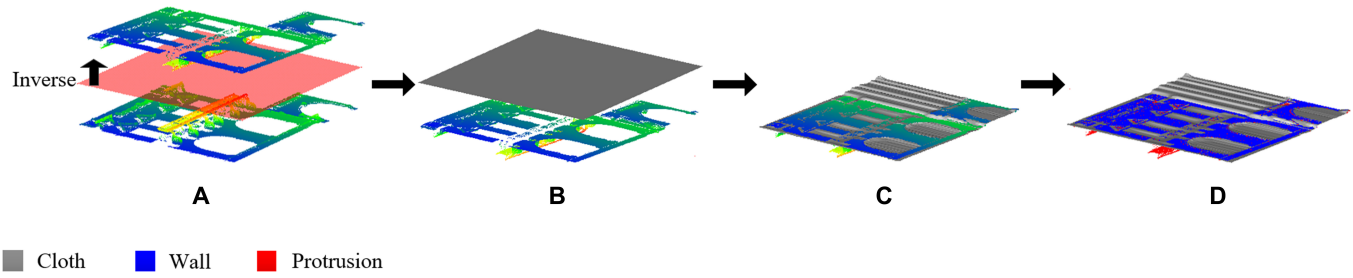

Fig. 7. Simple demonstration of CSF. (A) The natural-like scene is turned upside down. (B) A cloth (gray surface) is placed above the inverted (upside down) natural-like scene, and a wall surface is estimated by simulating the physical process of the collision between cloth and natural-like scene. (C) The wall surface is confirmed by the cloth. (D) The points inside and outside of the wall surface buffer are labeled as wall and protrusion points, respectively.

$$\theta y = \cos^{-1}\left[\frac{(x_b, z_b)\cdot(x_z, z_z)}{\left(\sqrt{x_b^2+z_b^2}\right)\times\left(\sqrt{x_z^2+z_z^2}\right)}\right] \quad (4)$$

where (x_b, y_b, z_b) and (x_z, y_z, z_z) are the coordinates of $\vec{n}_b$ and $\vec{n_z}$, respectively. According to R, the coordinates (x', y', z') of facade points after rotation are calculated as Eq. 5.

$$\begin{bmatrix} x' \\ y' \\ z' \end{bmatrix} = R \begin{bmatrix} x \\ y \\ z \end{bmatrix} \quad (5)$$

where (x, y, z) and (x', y', z') are the coordinates of facade points before and after rotation. Figure 6 shows an example of the facades before and after rotation. The facade after rotation is equivalent to the natural-like scene, where the protrusions are translated from the front to top of the wall.

Wall and protrusion separation

The separation problem is solved with existing ground filtering methods, after the facade is converted to the natural-like scene. Here, cloth simulation filter (CSF) is used as an example ground filtering method. CSF separates wall and protrusion points by simulating the physical process of cloth-touching objects. First, the natural-like scene is inverted (Fig. 7A), and a piece of cloth is placed above the inverted natural-like scene (Fig. 7B). Then, the shape of cloth is simulated by an external force operation followed by an internal force operation. The simulation process is performed iteratively until the shape of cloth no longer changes, and the cloth is considered as wall surface (Fig. 7C). Finally, wall and protrusion points are identified by comparing the height differences between facade points and wall surface. The detailed description of CSF is available in the literature [35,36].

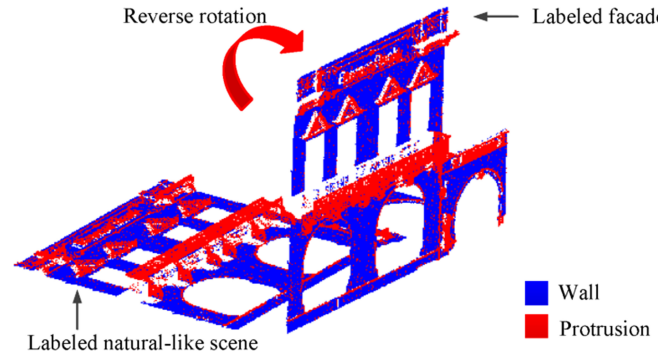

Fig. 8. An example of the restoration from natural-like scene to facade. The natural-like scene after a reverse rotation is restored to its original standing state.

Restoration from natural-like scene to facade

The labeled natural-like scene is restored to a facade using the inverse matrix R^{-1} of R. The coordinates of facade points after restoration are calculated as Eq. 6.

$$\begin{bmatrix} x \\ y \\ z \end{bmatrix} = R^{-1} \begin{bmatrix} x' \\ y' \\ z' \end{bmatrix} \quad (6)$$

where (x', y', z') and (x, y, z) are the coordinates of facade points before and after restoration. Figure 8 shows an example of the restoration from natural-like scene to facade. The natural-like scene after a reverse rotation has the same state as the original facade.

Parameter settings

There are 5 user-defined parameters in the proposed method, i.e., number of neighbor points k, grid resolution gr, step s, rigidness r, and height different Δh. k controls the accuracy of normal vectors and is set empirically. gr represents the horizontal distance between neighbor cloth particles, which controls how detailed the cloth describes walls. It is recommended

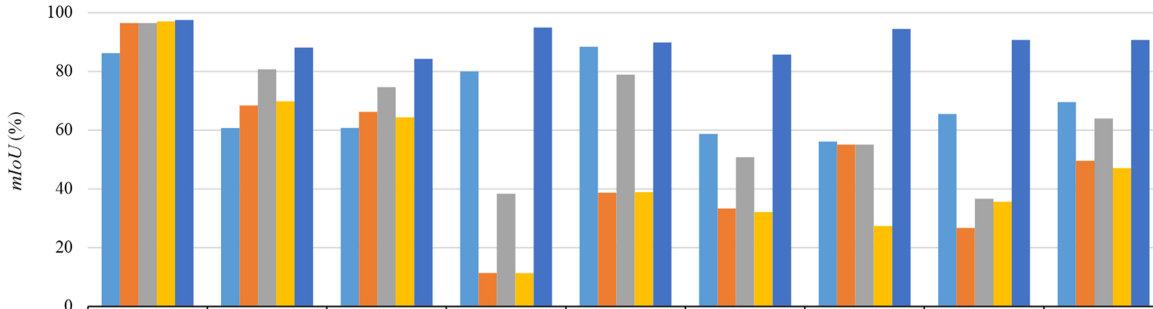

	Facade 1	Facade 2	Facade 3	Facade 4	Facade 5	Facade 6	Facade 7	Facade 8	Average
Region growing-based method	86.16	60.72	60.75	79.95	88.42	58.73	56.08	65.44	69.53
RANSAC-based method	96.48	68.43	66.17	11.36	38.74	33.29	55.05	26.65	49.52
Multi-pass RANSAC-based method	96.48	80.72	74.63	38.32	78.84	50.76	55.05	36.67	63.93
Hybrid method	97.06	69.81	64.38	11.29	38.84	32.12	27.42	35.61	47.07
The proposed method	97.52	88.06	84.27	94.94	89.86	85.70	94.49	90.72	90.70

Fig. 9. Quantitative comparison between different wall and protrusion separation methods in each sample.

that gr be set to the average point spacing of facade points. r represents the rigidness of cloth. If walls are planar, large rigidness cloth is selected ($r = 3$). If walls are smoothly curved or consists of multiple nonparallel planar parts, medium rigidness cloth is needed ($r = 2$). If walls consist of curved and planar parts, small rigidness cloth is set ($r = 1$) [35]. s is the descending height of cloth each time. Δh determines the final classification of facade points according to the height differences between facade points and wall surface. s and Δh should be less than the smallest protruding distance of protrusions. According to the above rules, the parameters in each facade are set, as listed in Table 2.

Experimental setup

Accuracy measures

Mean intersection over union (mIoU) was used to quantitatively assess the performance of the proposed method. The per-class IoU indicates the proportion of the intersection and union between the actual and reference points for wall and protrusion detection. IoU is calculated using Eq. 7 [37].

$$\text{IoU} = \frac{TP}{TP + FN + FP} \tag{7}$$

where TP, FN, and FP represent the numbers of the wall (protrusion) points correctly identified, the missing wall (protrusion) points, and the protrusion (wall) points mistakenly identified as wall (protrusion) points, respectively, when evaluating the performance of each method pertaining to the wall (protrusion) detection. The mIoU is the average of IoU values in wall and protrusion detection.

Comparative methods

The region growing-, RANSAC-, multipass RANSAC-based, and hybrid methods were implemented for the comparison with the proposed method [16,18,26,38]. To avoid improper parameter settings biasing the performance of the comparative methods, the parameters of the comparative methods were set by the fine-tuning method, and the parameter settings corresponding to the optimal results (i.e., the maximum mIoU values) were adopted. The fine-tuned parameters of the region growing-based method are the curvature c, the

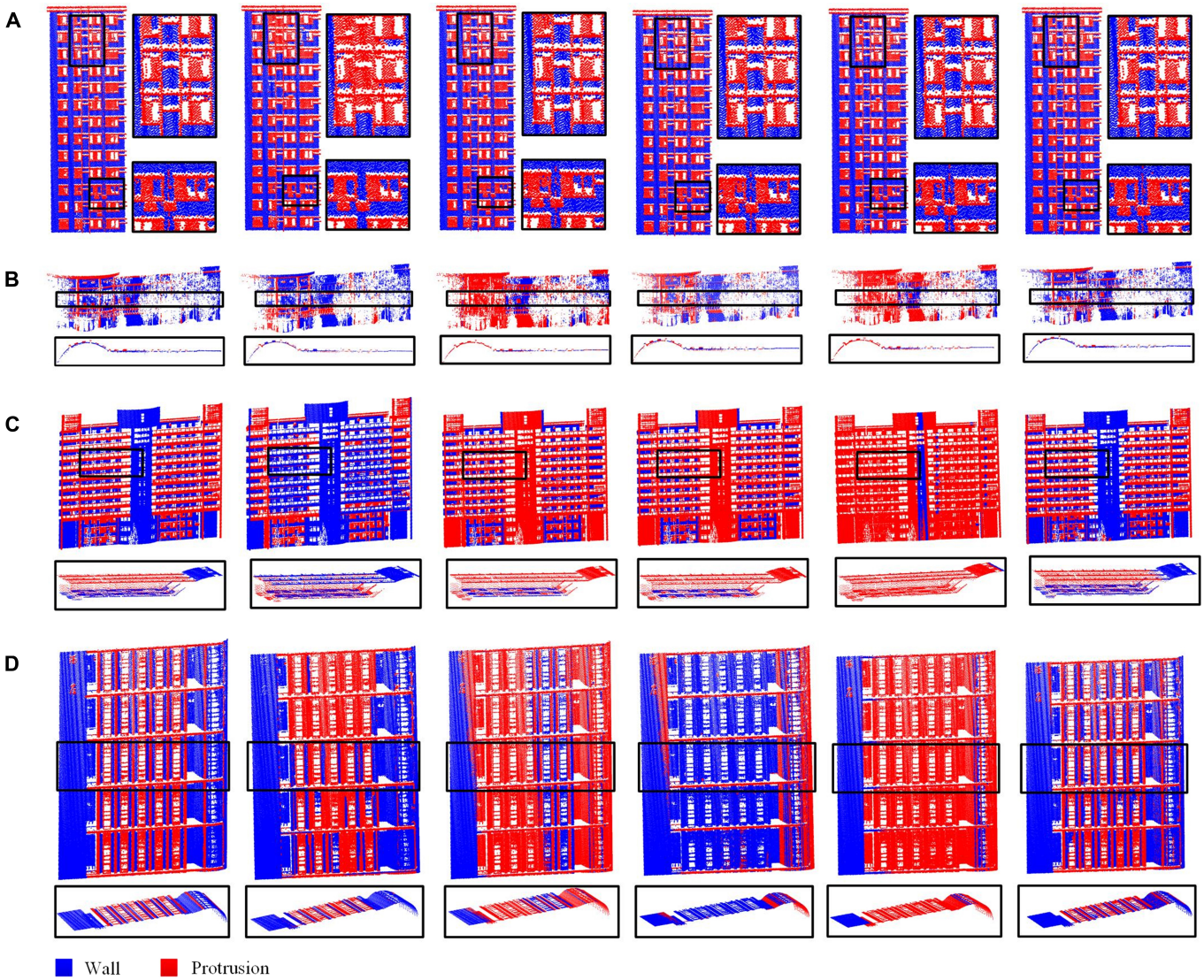

Fig. 10. Qualitative comparison between different methods in representative samples: (A) facade 1, (B) facade 6, (C) facade 7, and (D) facade 8. From the first to the last column: results of the reference, region growing-, RANSAC-, multipass RANSAC-based, hybrid, and proposed methods.

Table 2. Parameter settings of the proposed method.

Samples	k (point)	gr (m)	s (m)	r	Δh (m)
Facade 1	20	0.1	0.01	3	0.01
Facade 2	20	0.1	0.02	3	0.02
Facade 3	20	0.1	0.015	3	0.015
Facade 4	20	0.1	0.1	2	0.1
Facade 5	20	0.1	0.03	2	0.03
Facade 6	20	0.1	0.01	1	0.01
Facade 7	20	0.1	0.02	1	0.02
Facade 8	20	0.1	0.01	1	0.01

angle between the normal vectors of neighbor points θp, the angle between the normal vectors of point clusters and the z axis $\theta cluster$, and the number of points contained in each cluster *Ncluster*. c, θp, $\theta cluster$, and *Ncluster* were changed from 0.05 to 0.5, from 1° to 10°, from 3° to 30°, and from 100 to 1,000 points at intervals of 0.05, 1°, 3°, and 100 points, respectively. The fine-tuned parameter of the RANSAC-based method is the distances between facade points and detected plane d_p . We took the smallest protruding distance of protrusions in each facade as a center and selected the 10 nearest neighbor values as candidate protruding distances at intervals of 0.005 m. For example, the smallest protruding distance of protrusions in facade 1 is 0.01 m, and d_p was changed from 0.005 to 0.05 m. The fine-tuned parameters of the multipass RANSAC-based method are d_p and the maximum number of detected planes $N_{plane}^{\max}$. d_p was tuned in the same manner as the RANSAC-based method. $N_{plane}^{\max}$ was changed from 1 to 10 at intervals of 1. The fine-tuned parameters of the hybrid method include c, θp, $\theta cluster$, and d_p, which were tuned in the same manner as the region growing- and RANSAC-based methods. Table 3 provides the parameter settings of all the comparative methods.

Different ground filtering methods

To further verify the generalizability of the proposed methods, we also performed wall and protrusion separation in natural-like scenes using 3 classic ground filtering methods, including maximum slope filter (MSF) [39], progressive morphology filter (PMF) [40], and progressive triangular irregular network densification filter (PTDF) [41]. MSF and PMF were implemented using the C++ programming language, and PTDF was implemented using Terrisolid software.

Results

Accuracy of the proposed method

Table 4 illustrates the quantitative results of the proposed method in all 8 facade point clouds. The proposed method was accurate and robust to all facades, with a mean mIoU of 90.7% and a standard deviation (SD) of 4.37%. Meanwhile, the IoU and SD values of wall and protrusion detection were also satisfactory.

Comparison with other methods

The proposed method had the highest mIoU in each facade compared to the region growing-, RANSAC-, multipass RANSAC-based, and hybrid methods, as shown in Fig. 9. The mean mIoU values of the comparative methods and the proposed method were 69.53%, 49.52%, 63.93%, 47.07%, and 90.7%, respectively. The mIoU of the proposed method was obviously higher than the region growing-based method in the facades containing many small-sized point clusters (facades 1 to 4 and 6). Compared with the RANSAC-based method, the mIoU of the proposed method was obviously better in all facades other than facade 1. The wall of facade 1 consists of coplanar planar parts, while the walls of other facades are composed of noncoplanar planar and nonplanar parts. Although the mIoU of the multipass RANSAC-based method was improved compared to the RANSAC-based method in facades 2 to 6 and 8, it was still obviously lower than that of the proposed method in facades 4 to 6 and 8. The mIoU of the hybrid method was comparable to that of the RANSAC-based method in all facades. Note that

Table 3. Parameter settings of the comparative methods.

	Region growing-based method				RANSAC-based method	Multipass RANSAC-based method		Hybrid method			
Facades	c (°)	θp (°)	$\theta cluster$ (°)	*Ncluster* (points)	d_p (m)	d_p (m)	$N_{plane}^{\max}$	c (°)	θp (°)	$\theta cluster$ (°)	d_p (m)
1	0.1	9	15	200	0.045	0.035	1	0.25	8	3	0.05
2	0.2	3	3	900	0.05	0.035	2	0.15	4	3	0.05
3	0.15	9	3	500	0.05	0.045	3	0.2	9	3	0.04
4	0.15	10	3	500	0.125	0.125	5	0.15	10	3	0.125
5	0.25	8	15	700	0.055	0.045	4	0.2	10	3	0.055
6	0.2	8	12	200	0.05	0.05	5	0.15	7	3	0.05
7	0.15	5	6	400	0.05	0.05	1	0.05	3	3	0.05
8	0.2	5	3	400	0.05	0.05	5	0.15	7	3	0.045

when 2 methods have greater than 10% differences in mIoU, their difference in accuracy is stated as "obviously".

Figure 10 shows the visual results of wall and protrusion separation of 4 representative facades (i.e., facades 1 and 6 to 8). In facade 1, the region growing-based method misidentified many wall points as protrusion points. The RANSAC-, multipass RANSAC-based, hybrid, and proposed methods obtained similar visual results and outperformed the region growing-based method (Fig. 10A). In facade 6, the results of the region growing- and multipass RANSAC-based methods were superior to those of the RANSAC-based and hybrid methods especially in the nonplanar parts of the wall. In comparison, the result of the proposed method was the closest to the reference (Fig. 10B). In facade 7, the region growing-based method successfully separated most wall and protrusion points. The RANSAC- and multipass RANSAC-based methods obtained similar results, where only the planar parts of the wall were correctly identified. The hybrid method provided poor separation result, where almost all points were labeled as protrusion points. The result of the proposed method had a closer appearance to the reference than that of the region growing-based method especially in large-sized protrusions, as shown in the enlarged view of Fig. 10C. In facade 8, the region growing-based method provided better results than the RANSAC-, multipass RANSAC-based, and hybrid methods. The proposed method outperformed the region growing-based method especially in the identification of large-sized protrusions (Fig. 10D).

Generalizability of the proposed method

The mIoU values of different ground filtering methods (including MSF, PMF, and PTDF) are provided in Fig. 11. All methods achieved high accuracy (mean mIoU values > 80%), and the quantitative results of these methods were substantially higher than the above traditional separation methods (Figs. 9 and 10). The visualization results of the methods in 4 representative samples (i.e., facades 1 and 6 to 8) illustrated the effectiveness of different ground filtering methods for wall and protrusion separation (Fig. 12). Therefore, the proposed method had strong generality because existing filtering methods could be all directly applied.

Table 4. Quantitative results of the proposed method.

Facades	IoU of wall detection (%)	IoU of protrusion detection (%)	mIoU (%)
1	97.88	97.17	97.52
2	92.09	84.04	88.06
3	82.05	86.5	84.27
4	99.92	89.97	94.94
5	93.92	85.8	89.86
6	90.86	80.53	85.7
7	95.22	93.76	94.49
8	92.9	88.54	90.72
Average	93.11	88.29	90.7
SD	5.03	4.99	4.37

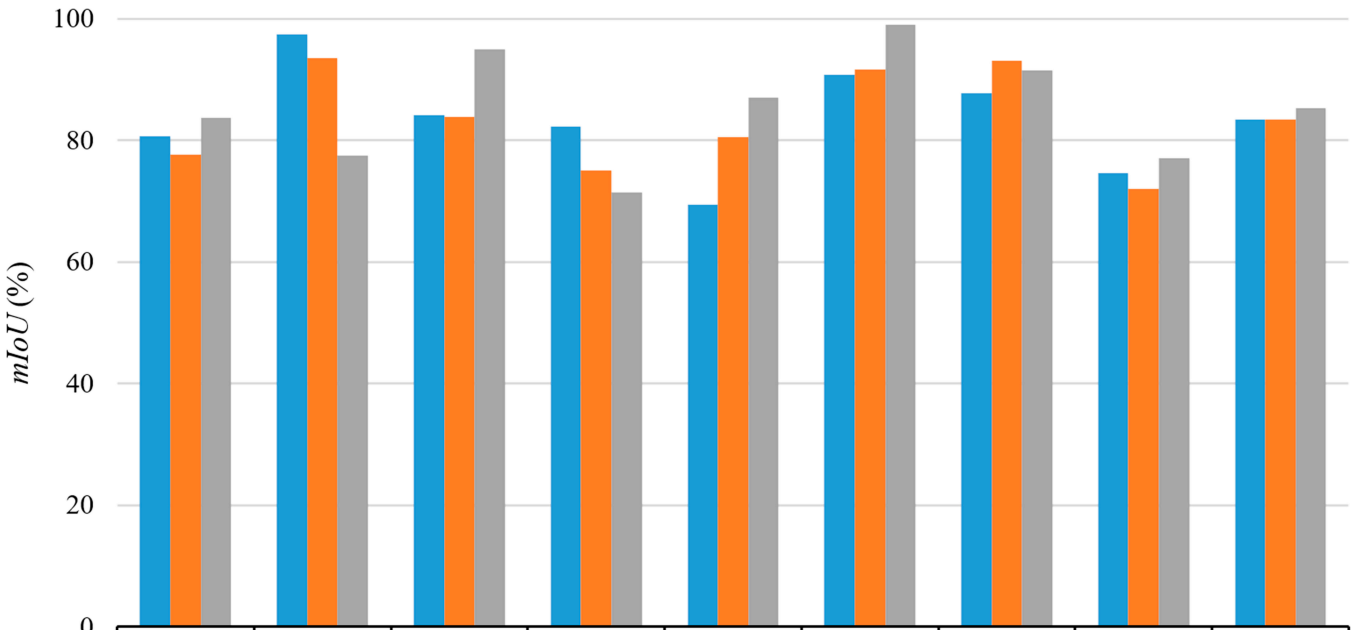

	Facade 1	Facade 2	Facade 3	Facade 4	Facade 5	Facade 6	Facade 7	Facade 8	Average
MSF	80.71	97.44	84.22	82.33	69.45	90.88	87.74	74.58	83.42
PMF	77.73	93.64	83.96	75.07	80.61	91.7	93.08	72.03	83.48
PTDF	83.75	77.57	94.99	71.52	87.01	99.06	91.54	77.09	85.32

Fig. 11. Quantitative results of wall and protrusion separation using different ground filtering methods.

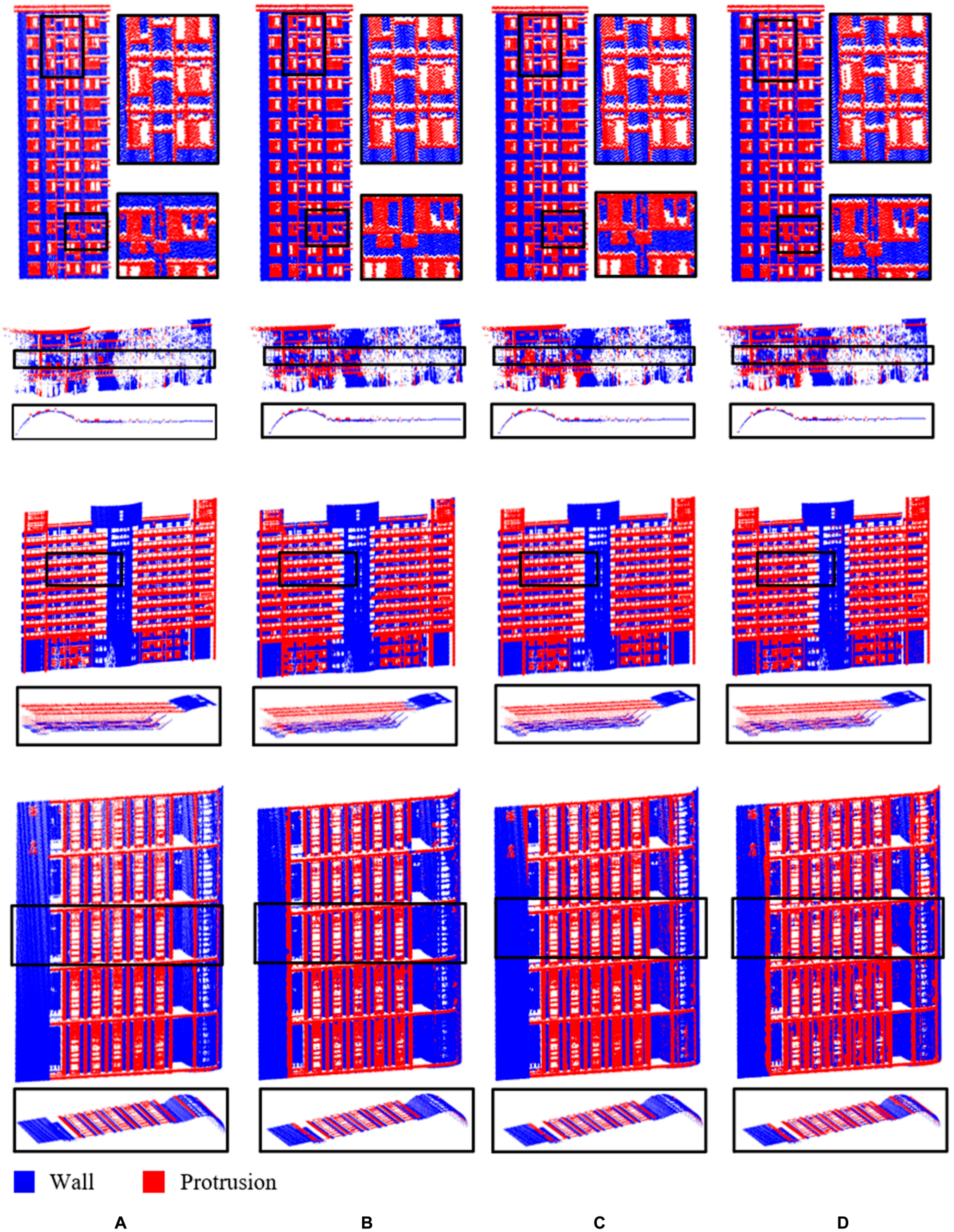

Fig. 12. Qualitative results of wall and protrusion separation using different ground filtering methods: (A) reference, (B) MSF, (C) PMF, and (D) PTDF.

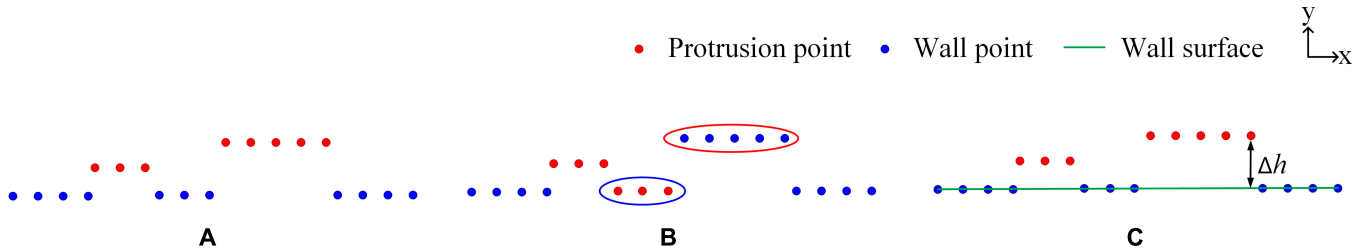

Fig. 13. Simple demonstration of the superiority of the proposed method over the region growing-based method: the results of (A) reference, (B) the region growing-based method, and (C) the proposed method. Note that facade point clouds are represented in the top view, and the misidentified wall and protrusion points are marked with blue and red ellipses. Δh represents the z-value differences between points and wall surface.

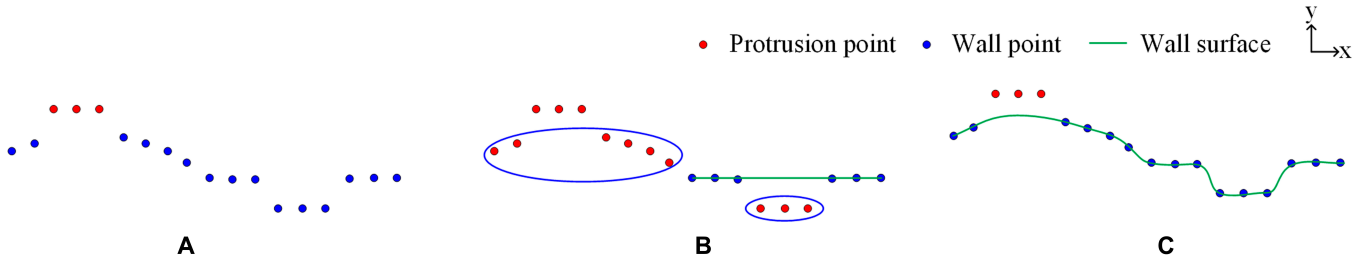

Fig. 14. Simple demonstration of the superiority of the proposed method over the RANSAC-based method: the results of (A) reference, (B) the RANSAC-based method, and (C) the proposed method. Note that facade point clouds are represented in the top view, and misidentified wall points are marked with blue ellipses.

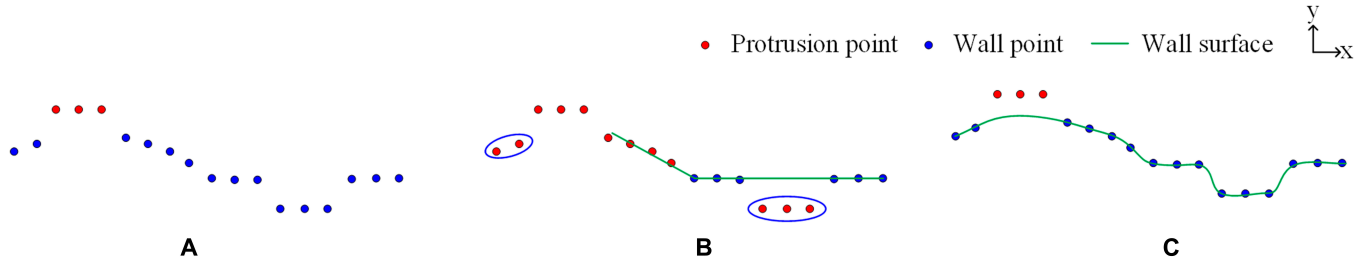

Fig. 15. Simple demonstration of the superiority of the proposed method over the multipass RANSAC-based method: the results of (A) reference, (B) the multipass RANSAC-based method, and (C) the proposed method. Note that facade point clouds are represented in the top view, and the misidentified wall points are marked with blue ellipses.

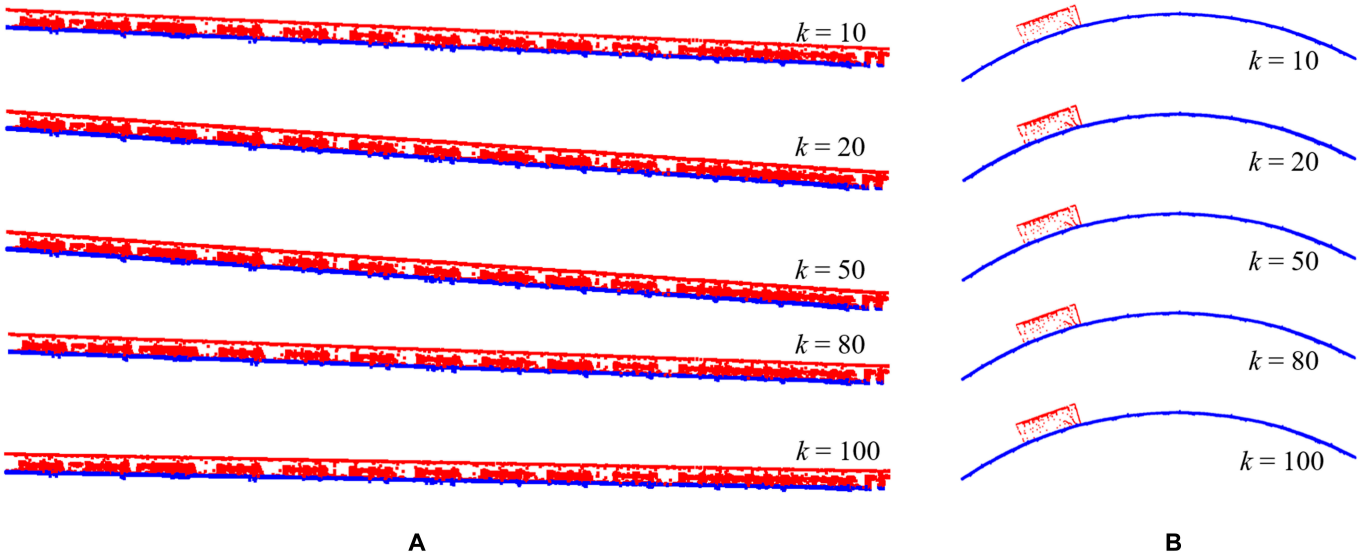

Fig. 16. The natural-like scenes generated with different k values. Here, the experiment was performed in (A) a simple facade and (B) a complex facade.

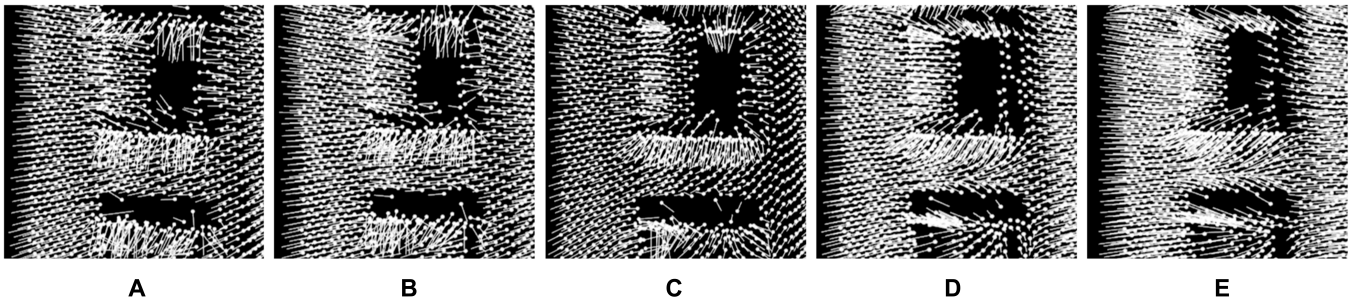

Fig. 17. The normal vectors of facade points calculated using different k values: (A) $k = 10$, (B) $k = 20$, (C) $k = 50$, (D) $k = 80$, and (E) $k = 100$.

Discussion

Overall performance of the proposed method

To overcome the limitation that the walls and protrusions in only specific types of facades can be accurately separated by the traditional methods, we presented a more generic separation method. Overall, the proposed method not only achieved high accuracy in various facade conditions but was also worth popularizing since existing ground filtering methods can be directly applied. How to transform the wall and protrusion separation problem to a ground filtering problem is the fundamental premise for the proposed method. The transformation is essentially to ensure that the protruding directions of protrusions relative to walls are vertical upward because ground filtering methods usually formulate the prior knowledge as rules using the z-axis direction as a benchmark, i.e., the z values of nonground objects are greater than those of ground in local regions. We achieved the transformation by rotating facade normal vectors to be parallel to the z axis. The accurate separation results and the fact that the existing filtering methods can be all applied demonstrated the effectiveness of the transformation (Figs. 9 to 12).

Performance comparison

The comparison results showed that the accuracy of the proposed method was substantially higher than the comparative methods. Specifically, the proposed method substantially reduced the identification errors of small-sized walls and large-sized protrusions compared to the region growing-based method (Figs. 9 and 10) due to the use of more reliable prior knowledge. A top view representation of facade point cloud was used to explain the reason for the difference in performance of the 2 methods, as shown in Fig. 13. The point clusters of small-sized wall and large-sized protrusion were misidentified by the region growing-based method (see blue and red ellipses in Fig. 13B). The proposed method was insensitive to the sizes of point cluster, which separates walls and protrusions based on the z-value differences (Δh) between facade points and wall surfaces. Thus, the small-sized walls and large-sized protrusions can be accurately identified by the proposed method, as shown in Fig. 13C.

The proposed method had a substantial advantage compared with the RANSAC-based method in the facades, where walls consist of noncoplanar planar and nonplanar parts (Figs. 9 and 10). As shown by the example in Fig. 14, the noncoplanar planar and nonplanar parts of the wall were misidentified as protrusions by the RANSAC-based method (see blue ellipses in Fig. 14B) because the wall can only be represented by a plane. On the contrary, the proposed method can accurately estimate the wall surface, identifying the noncoplanar planar and nonplanar parts of the wall, as shown in Fig. 14C.

The multipass RANSAC-based method performed better than the RANSAC-based method in facades, where the walls include noncoplanar point clusters (Figs. 9 and 10). However, its accuracy was always lower than the proposed method. As shown by the example in Fig. 15, the small-sized wall point clusters were still incorrectly identified as protrusions (see blue ellipses in Fig. 15B), since the wall surface in these areas cannot be accurately represented by the RANSAC plane fitting. However, the proposed method overcomes the problem, resulting in a more accurate separation result.

Parameter sensitivity

Parameter k is the number of neighbor points for calculating the normal vectors of facade points, which may determine whether facades can be effectively transformed into natural-like scenes. To assess the sensitivity of the proposed method to k, we took a simple facade and a complex facade as examples (i.e., facades 1 and 4) to calculate the normal vectors of facade points using different k values, changing from 10 to 100 points at intervals of 10 points. Figure 16 shows the natural-like scenes corresponding to facades 1 and 4 when k values are equal to 10, 20, 50, 80, and 100 points. The natural-like scenes had similar appearances, indicating that the transformation from facade to natural-like scene step was insensitive to k.

To explore the possible reason why the transformation is insensitive to k, we visualized the normal vector at each point of the local area in facade 1, as shown in Fig. 17. The normal vectors at wall and protrusion points were approximately perpendicular to the facade, respectively, while the normal vectors at the edge points between wall and protrusion were strongly variable under different k values. The negative effect of edge points is limited because of its small proportion in facade points. Thus, the transformation from facade to natural-like scene step is seldom affected by the setting of k.

Conclusion

This study presents a novel wall and protrusion separation method. Its main principle is to convert the wall and protrusion separation problem to a ground filtering problem and to separate walls and protrusions using ground filtering methods. Comprehensive experiments demonstrated that the proposed method performed well in various facade conditions and substantially outperformed traditional separation methods. Moreover, existing ground filtering methods can be all directly used to separate walls and protrusions. It indicated that the proposed method was general and effective in terms of

facade conditions and applications, providing a useful tool for semantic facade reconstruction.

Although the proposed method exhibits higher performance than the traditional separation methods, it has a limitation as well. The proposed method might not work well in the facades that include particularly few wall points. An interesting topic for future research will be to consider whether a combination of multisource data can be utilized to overcome the limitation.

Acknowledgments

Funding: This work was supported by the National Natural Science Foundation of China, grant nos. 41971380 and 41671414. This work was also supported by Guangxi Natural Science Fund for Innovation Research Team (grant no. 2019JJF50001), the Open Fund of State Key Laboratory of Remote Sensing Science (grant no. OFSLRSS201920), and leading talents of Guangdong Pearl River Talent Program (grant no. 2021CX02S024). **Competing interests:** The authors declare that they have no competing interests. **Author contributions:** S.C., W.Z., and H.F. conceived the ideas, designed the experiment, and wrote the manuscript. S.Y. participated in the data preprocessing. S.Z., W.Z., and J.S. revised the manuscript. G.Y., A.L., and G.Z. provided valuable suggestions.

Data Availability

The data that support this study are available from the corresponding author upon reasonable request.

References

1. Vo A-V, Truong-Hong L, Laefer DF. Aerial laser scanning and imagery data fusion for road detection in city scale. Paper presented at: Proceedings of the 2015 IEEE International Geoscience and Remote Sensing Symposium (IGARSS); 2015 Jul; Milan, Italy.
2. Deng H, Zhang L, Mao X, Qu H. Interactive urban context-aware visualization via multiple disocclusion operators. *IEEE Trans Vis Comput Graph*. 2016;22(7):1862–1874.
3. Li Y, Zheng Q, Sharf A, Cohen-Or D, Chen B, Mitra NJ. 2D-3D fusion for layer decomposition of urban facades. Paper presented at: Proceedings of the 2011 International Conference on Computer Vision; 2011 Nov; Barcelona, Spain.
4. Wang Y, Fan H, Zhou G. Reconstructing facade semantic models using hierarchical topological graphs. *Trans GIS*. 2020;24(4):1073–1097.
5. Fan H, Wang Y, Gong J. Layout graph model for semantic façade reconstruction using laser point clouds. *Geo-spatial Inform Sci*. 2021;24(3):403–421.
6. Yang L, Sheng Y, Wang B. 3D reconstruction of building facade with fused data of terrestrial LiDAR data and optical image. *Optik*. 2016;127(4):2165–2168.
7. Brito MC, Freitas S, Guimarães S, Catita C, Redweik P. The importance of facades for the solar PV potential of a Mediterranean City using LiDAR data. *Renew Energy*. 2017;111:85–94.
8. Martínez-Rubio A, Sanz-Adan F, Santamaría-Peña J, Martínez A. Evaluating solar irradiance over facades in high building cities based on LiDAR technology. *Appl Energy*. 2016;183:133–147.
9. Haghighatgou N, Daniel S, Badard T. A method for automatic identification of openings in buildings facades based on mobile LiDAR point clouds for assessing impacts of floodings. *Int J Appl Earth Obs Geoinf*. 2022;108:102757.
10. Becker S. Generation and application of rules for quality dependent façade reconstruction. *ISPRS J Photogramm Remote Sens*. 2009;64(6):640–653.
11. Tang P, Huber D, Akinci B, Lipman R, Lytle A. Automatic reconstruction of as-built building information models from laser-scanned point clouds: A review of related techniques. *Autom Constr*. 2010;19(7):829–843.
12. Xia S, Wang R. Façade separation in ground-based LiDAR point clouds based on edges and windows. *IEEE J Sel Top Appl Earth Observ Remote Sens*. 2019;12(3):1041–1052.
13. Xia S, Wang R. Semiautomatic construction of 2-D façade footprints from mobile LiDAR data. *IEEE Trans Geosci Remote Sens*. 2019;57(6):4005–4020.
14. Martínez J, Soria-Medina A, Arias P, Buffara-Antunes AF. Automatic processing of terrestrial laser scanning data of building façades. *Autom Constr*. 2012;22:298–305.
15. Riemenschneider H, Krispel U, Thaller W, Donoser M, Havemann S, Fellner D, Bischof H. Irregular lattices for complex shape grammar facade parsing. Paper presented at: Proceedings of the 2012 IEEE Conference on Computer Vision and Pattern Recognition; 2012 Jun 16–21; Providence, USA.
16. Wan G, Sharf A. Grammar-based 3D facade segmentation and reconstruction. *Comput Graph*. 2012;36(4):216–223.
17. Friedman SF, Stamos I. Online detection of repeated structures in point clouds of urban scenes for compression and registration. *Intl J Comput Vision*. 2013;102(1-3):112–128.
18. Li Z, Zhang L, Mathiopoulos PT, Liu F, Zhang L, Li S, Liu H. A hierarchical methodology for urban facade parsing from TLS point clouds. *ISPRS J Photogramm Remote Sens*. 2017;123:75–93.
19. Hamid-Lakzaeian F. Point cloud segmentation and classification of structural elements in multi-planar masonry building facades. *Autom Constr*. 2020;118:103232.
20. Feng Y, Xiao Q, Brenner C, Peche A, Yang J, Feuerhake U, Sester M. Determination of building flood risk maps from LiDAR Mobile mapping data. *Comput Environ Urban Syst*. 2022;93:101759.
21. Klimkowska A, Cavazzi S, Leach R, Grebby S. Detailed three-dimensional building façade reconstruction: A review on applications, data and technologies. *Remote Sens*. 2022;14(11):2579.
22. Wang Y, Ma Y, Zhu A, Zhao H, Liao L. Accurate facade feature extraction method for buildings from three-dimensional point cloud data considering structural information. *ISPRS J Photogramm Remote Sens*. 2018;139:146–153.
23. Xu Y, Tuttas S, Hoegner L, Stilla U. Voxel-based segmentation of 3D point clouds from construction sites using a probabilistic connectivity model. *Pattern Recogn Lett*. 2018;102:67–74.
24. Zolanvari SMI, Laefer DF, Natanzi AS. Three-dimensional building façade segmentation and opening area detection from point clouds. *ISPRS J Photogramm Remote Sens*. 2018;143:134–149.
25. Hamid-Lakzaeian F. Structural-based point cloud segmentation of highly ornate building façades for computational modelling. *Autom Constr*. 2019;108:102892.
26. Pu S, Vosselman G. Knowledge based reconstruction of building models from terrestrial laser scanning data. *ISPRS J Photogramm Remote Sens*. 2009;64(6):575–584.
27. Weinmann M, Jutzi B, Hinz S, Mallet C. Semantic point cloud interpretation based on optimal neighborhoods, relevant features and efficient classifiers. *ISPRS J Photogramm Remote Sens*. 2015;105:286–304.
28. Dong Z, Yang B, Hu P, Scherer S. An efficient global energy optimization approach for robust 3D plane segmentation of point clouds. *ISPRS J Photogramm Remote Sens*. 2018;137:112–133.

29. Boulaassal H, Landes T, Grussenmeyer P. Automatic extraction of planar clusters and their contours on building façades recorded by terrestrial laser scanner. *Int J Archit Comput*. 2009;7(1):1–20.
30. Iman Zolanvari SM, Laefer DF. Slicing method for curved façade and window extraction from point clouds. *ISPRS J Photogramm Remote Sens*. 2016;119:334–346.
31. Nan L, Sharf A, Zhang H, Cohen-Or D, Chen B. SmartBoxes for interactive urban reconstruction. *ACM Trans Graph*. 2010;29(4):1–10.
32. Friedman S, Stamos I. Real time detection of repeated structures in point clouds of urban scenes. Paper presented at: Proceedings of the 2011 International Conference on 3D Imaging, Modeling, Processing, Visualization and Transmission; 2011 May; Hangzhou, China.
33. Liang X, Litkey P, Hyyppa J, Kaartinen H, Vastaranta M, Holopainen M. Automatic stem mapping using single-scan terrestrial laser scanning. *IEEE Trans Geosci Remote Sens*. 2012;50(2):661–670.
34. Wang R, Ferrie FP, Macfarlane J. A method for detecting windows from mobile Lidar data. *Photogramm Eng Remote Sens*. 2012;78(11):1129–1140.
35. Zhang W, Qi J, Wan P, Wang H, Xie D, Wang X, Yan G. An easy-to-use airborne LiDAR data filtering method based on cloth simulation. *Remote Sens*. 2016;8(6):501.
36. Cai S, Zhang W, Liang X, Wan P, Qi J, Yu S, Yan G, Shao J. Filtering airborne LiDAR data through complementary cloth simulation and progressive TIN densification filters. *Remote Sens*. 2019;11(9):1037.
37. Xiao A, Yang X, Lu S, Guan D, Huang J. FPS-net: A convolutional fusion network for large-scale LiDAR point cloud segmentation. *ISPRS J Photogramm Remote Sens*. 2021;176:237–249.
38. Canaz Sevgen S, Karsli F. An improved RANSAC algorithm for extracting roof planes from airborne Lidar data. *Photogram Rec*. 2020;35:40–57.
39. Vosselman G. Slope based filtering of laser altimetry data. *Intl Arch Photogramme Remote sens*. 2000;33:935–942.
40. Zhang K, Chen SC, Whitman D, Shyu ML, Yan J, Zhang C. A progressive morphological filter for removing nonground measurements from airborne LIDAR data. *IEEE Trans Geosci Remote Sens*. 2003;41(4):872–882.
41. Axelsson P. DEM generation from laser scanner data using adaptive TIN models. Paper presented at: International Archives of Photogrammetry and Remote Sensing; 2000.